MNRAS 000, 1–16 (2021) Preprint 29 March 2021 Compiled using MNRAS LATEX style file v3.0

Thermal Formaldehyde Emission in NGC 7538 IRS 1

Onic I. Shuvo,[1,2]★ E. D. Araya,[2,3]† W. S. Tan,[2] P. Hofner,[3]‡
S. Kurtz,[4] Y. M. Pihlström,[5]§ and I. M. Hoffman[6]

[1]*Department of Physics and Astronomy, George Mason University, 4400 University Drive, Fairfax, VA 22030, USA.*
[2]*Physics Department, Western Illinois University, 1 University Circle, Macomb, IL 61455, USA.*
[3]*New Mexico Institute of Mining and Technology, Physics Department, 801 Leroy Place, Socorro, NM 87801, USA.*
[4]*Instituto de Radioastronomía y Astrofísica, Universidad Nacional Autónoma de México, Apdo. Postal 3-72, 58090, Morelia, Michoacán, Mexico.*
[5]*Department of Physics and Astronomy, University of New Mexico, 210 Yale Blvd. NE, Albuquerque, NM 87131, USA.*
[6]*Quest University, 3200 University Boulevard, Squamish, British Columbia V8B0N8, Canada.*

Accepted 2021 March 19. Received 2021 March 18; in original form 2020 October 16.

ABSTRACT

Spectral lines from formaldehyde (H_2CO) molecules at cm wavelengths are typically detected in absorption and trace a broad range of environments, from diffuse gas to giant molecular clouds. In contrast, thermal emission of formaldehyde lines at cm wavelengths is rare. In previous observations with the 100 m Robert C. Byrd Green Bank Telescope (GBT), we detected 2 cm formaldehyde emission toward NGC 7538 IRS1 – a high-mass protostellar object in a prominent star-forming region of our Galaxy. We present further GBT observations of the 2 cm and 1 cm H_2CO lines to investigate the nature of the 2 cm H_2CO emission. We conducted observations to constrain the angular size of the 2 cm emission region based on a East-West and North-South cross-scan map. Gaussian fits of the spatial distribution in the East-West direction show a deconvolved size (at half maximum) of the 2 cm emission of $50'' \pm 8''$. The 1 cm H_2CO observations revealed emission superimposed on a weak absorption feature. A non-LTE radiative transfer analysis shows that the H_2CO emission is consistent with quasi-thermal radiation from dense gas ($\sim 10^5$ to 10^6 cm^{-3}). We also report detection of 4 transitions of CH_3OH (12.2, 26.8, 28.3, 28.9 GHz), the (8,8) transition of NH_3 (26.5 GHz), and a cross-scan map of the 13 GHz SO line that shows extended emission ($> 50''$).

Key words:
stars: formation — ISM: molecules — radio lines: ISM — ISM: individual (NGC 7538)

1 INTRODUCTION

Formaldehyde is a tracer of high density gas in high-mass star forming regions and it is a reliable density probe in Galactic molecular clouds (e.g., Mangum et al. 2008, Ginsburg et al. 2011). The rotational levels of ortho-formaldehyde (H_2CO) are split in doublets, commonly known as K-doublets. The K-doublet lines from the three lowest H_2CO rotational energy levels correspond to wavelengths of 6, 2, and 1 cm (e.g., Mangum & Wootten 1993, Thaddeus 1972).

While thermal emission of high-frequency formaldehyde transitions has been detected in high-mass star forming regions (e.g., Ceccarelli et al. 2003), thermal emission of the lowest K-doublet transitions is rare (e.g., Evans et al. 1975b; Araya et al. 2006a). At present, thermal 6 cm H_2CO emission has been detected only toward the Orion BN/KL region (e.g., Araya et al. 2006b). Galactic quasi-thermal emission of the 2 cm transition has been reported toward a few sources (Orion-KL, OMC-2, ρ Oph B, DR 21(OH), and three regions in W51; e.g, Ginsburg et al. 2016, Johnston et al. 1984, and references therein).[1] Thermal emission at 1 cm has been found toward 17 sources (McCauley et al. 2011). In contrast, formaldehyde masers have only been unambiguously detected in the 6 cm

★ E-mail: oshuvo@masonlive.gmu.edu
† E-mail: ed-araya@wiu.edu
‡ Adjunct Astronomer at the National Radio Astronomy Observatory, 1003 Lopezville Road, Socorro, NM 87801, USA.
§ Adjunct Astronomer at the National Radio Astronomy Observatory, 1003 Lopezville Road, Socorro, NM 87801, USA.

[1] We use the term *quasi-thermal* to refer to gas in between a state dominated by non-LTE excitation resulting in anomalous absorption ($T_{ex} < T_{CMB}$ in the low-density regime; e.g., Evans et al. 1975a) and LTE excitation dominated by molecular collisions (high-density regime).

transition (e.g., Chen et al. 2017b, Ginsburg et al. 2015, Araya et al. 2007b, Hoffman et al. 2003)[2]. Currently, 10 Galactic regions are know to harbor 6 cm masers (Andreev et al. 2017; Chen et al. 2017b), one of them is NGC 7538 – the region where 6 cm H_2CO masers were first confirmed (see review by Araya et al. 2007b).

NGC 7538 is an active site of high-mass star formation located at a distance of 2.65±0.12 kpc (Moscadelli et al. 2009). This region is one of the richest maser sources known (e.g., Galván-Madrid et al. 2010). Over a dozen different molecular maser transitions have been found in NGC 7538, including one of the rare 6 cm H_2CO masers (e.g., Araya et al. 2007a).

Using the 100 m Robert C. Byrd Green Bank Telescope (GBT), we detected 2 cm H_2CO emission toward NGC 7538 IRS 1 (Andreev et al. 2017). This emission was independently detected by Chen et al. (2017a). Given the non-detection of a 2 cm maser in interferometric observations (Hoffman et al. 2003), Chen et al. (2017a) argued that the 2 cm H_2CO emission in NGC 7538 IRS 1 is a variable maser, noting that variability has been detected in the 6 cm H_2CO maser in the same source (e.g., Andreev et al. 2017).

In this work, we present GBT observations of the 2 cm and 1 cm H_2CO transitions to investigate the nature of the 2 cm emission[3]. Depending on whether the emission is thermal or maser, the line would provide information on completely different scales, from tens of a.u.'s in the case of masers, to sub-pc structures in the case of thermal emission. In particular, if the 2 cm H_2CO emission is thermal, it would trace a connection between the large-scale molecular cloud in NGC 7538 and the molecular core hosting the IRS1 star formation site.

2 OBSERVATIONS

2.1 2 cm H_2CO

Observations of the 2 cm H_2CO transition in NGC 7538 were conducted with the GBT in November 2008. We observed the J_{KaKc}=2_{11}-2_{12} transition of formaldehyde (ν_0=14.488480 GHz, H_2CO 2 cm line)[4] with a bandwidth (BW) of 12.5 MHz observed in frequency switching mode (5 minutes per scan) that resulted in an effective bandwidth of 6.25 MHz (~130 km s^{-1}), 9 level sampling, 8192 channels and final channel separation of 21.3 kHz (0.442 km s^{-1}) after smoothing. Given the capabilities of the GBT spectrometer, we conducted observations using additional independent bands (spectral windows) tuned to the J_K = 2_0-3_{-1} E transition of CH_3OH (12.178593 GHz) and the N_J = 2_1-1_1 transition of SO (13.043814 GHz). The system temperature was approximately 30 K. A calibration diode was used to set the antenna temperature scale, and flux density calibration was done using the telescope gain values provided by the observatory in the GBTIDL[5] software package. We observed 3C48 in position switching mode to check the flux density calibration; we measured S_ν = 1.9 Jy at 14.8 GHz, which agrees within 10% with the expected value of 1.74 Jy[6]. Based on the pointing observations of 3C48, we measured a half-power beam width (HPBW) of 52″ at the frequency of the 2 cm H_2CO transition.

To investigate the angular size of the 2 cm H_2CO emission region and measure its brightness temperature, we obtained a 13-point (East-West, North-South) cross-scan map; the pointings were offset in the RA and Dec directions by ±27″, ±54″, and ±108″ with respect to the location of NGC 7538 IRS1 (R.A= $23^h13^m45.36^s$ and Dec= +61° 28′10.45″, J2000)[7].

2.2 1 cm H_2CO

We also observed the J_{KaKc}=3_{12}-3_{13} transition of formaldehyde (ν_0=28.974804 GHz, 1 cm H_2CO line) with the GBT on 30 October 2008. The spectrometer was used with a 50 MHz BW (~500 km s^{-1}), 9 level sampling, 8192 channels and final channel separation of 18.3 kHz (0.190 km s^{-1}) after smoothing. In the spectral window of the 1 cm H_2CO line, the J_K = 8_2-9_1 A^- transition of CH_3OH (28.969942 GHz) was also included[8]. Three additional spectral windows were used to simultaneously observe the (J,K) = (8,8) NH_3 (26.518981 GHz) line, and two transitions 12_2-12_1 E (26.847205 GHz) and 4_0-3_1 E (28.316031 GHz) of CH_3OH. The HPBW of the telescope at 29 GHz is ~26″.

The observation procedure was position-switching (ON-OFF mode) with 2 minutes on both ON and OFF (reference) positions per scan. We obtained 12 scans of NGC 7538 IRS1. The reference position was set to match the azimuth-elevation path tracked by the telescope during the corresponding 2 minutes ON-source observations. The system temperature was approximately 45 K. Calibration and data reduction were done using GBTIDL. We observed the quasars 3C48 and 2148+6107 for pointing and system checking. We measured a 3C48 flux density of S_ν = 0.92 Jy at 29 GHz, which agrees within 12% with the expected value of 0.82 Jy[6]. The pointing errors are estimated to be ~ 5″ in both RA and Dec based on the observations of 2148+6107.

3 RESULTS

Figure 1 shows the emission and absorption spectra of the three lowest K-doublet transitions of H_2CO towards NGC 7538 IRS1. The 1 cm and 2 cm H_2CO spectra are from the observations reported in this work, while the 6 cm H_2CO spectrum is from GBT observations reported by Araya et al. (2007a). Spectra of the other molecular transitions observed in this work are shown in Figures 2 and 3.

As mentioned above, we conducted cross-scan observations of 2 cm H_2CO, 12.2 GHz CH_3OH and 13.044 GHz SO transitions, simultaneously. The spectra of the 2 cm H_2CO cross-scan are shown in Figure 4. To explore the distribution of 2 cm H_2CO in the context of the IR and radio continuum environment in NGC 7538 IRS1, we

[2] Chen et al. (2017a) reported possible 2 cm H_2CO emission lines toward G23.01−0.41 and G29.96−0.02, in addition to NGC 7538; see below.

[3] Preliminary results from this work were presented at a conference by Yuan et al. (2011).

[4] Spectroscopy information in this paper is from Splatalogue (http://www.cv.nrao.edu/php/splat/) and the NIST Lovas catalog (https//physics.nist.gov/cgi-bin/micro/table5/start.pl), unless indicated otherwise.

[5] IDL (Interactive Data Language) is a trademark of Harris Geospatial Corp.

[6] https://www.vla.nrao.edu/astro/calib/manual/fluxscale.html

[7] Given the HPBW of the telescope, our IRS1 pointing also includes IRS2 and IRS3, e.g., Akabane et al. (1992).

[8] Rest frequency from the JPL catalog (https://spec.jpl.nasa.gov/ftp/pub/catalog/catform.html) as listed at the time of the observations, which was also used by McCauley et al. (2011). This frequency differs by 12 kHz with respect to the rest frequency reported in the Lovas catalog.

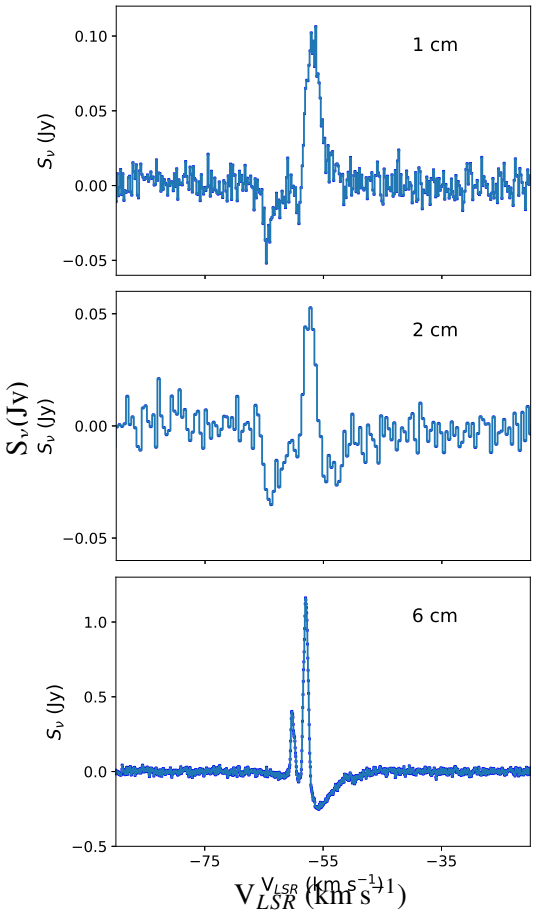

Figure 1. Spectra of 1 cm, 2 cm and 6 cm H_2CO transitions toward NGC 7538 IRS1. Note the detection of emission and absorption in all transitions. The data shown in the figure are available as Supporting Information.

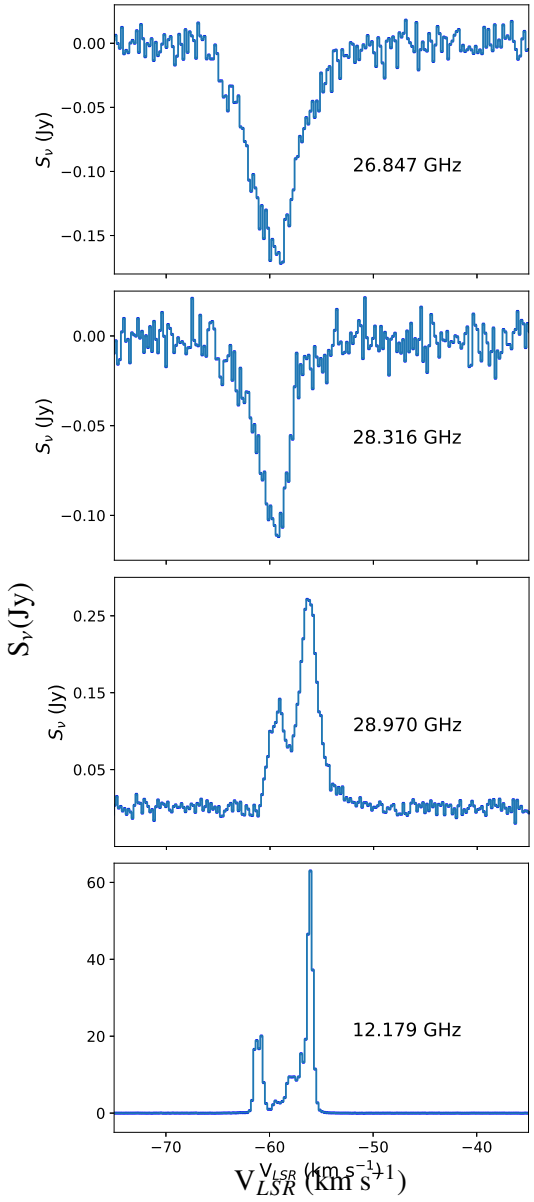

Figure 2. Detection of CH_3OH transitions toward NGC 7538 IRS1. Two transitions show absorption (top panels; 26.847 GHz and 28.316 GHz) and two transitions show emission lines (lower panels; 28.970 GHz and 12.178 GHz). The data shown in the figure are available as Supporting Information.

show the 2 cm H_2CO spectra superimposed with a Spitzer/IRAC[9] image and 6 cm VLA continuum from the NRAO image archive[10].

The detections were fit with Gaussian profiles; Figures 5 to 8 show the Gaussian fits of all 13 cross-scan pointings (East-West, North-South) of the 2 cm H_2CO, 12.2 GHz CH_3OH, and 13.044 GHz SO observations. The line parameters of 2 cm H_2CO observations from the free fit are listed in Table 1, whereas the line parameters from the fit after constraining the peak absorption velocities are listed in Table 2 (see Section 4.1 for details). The free fit line parameters of 12.2 GHz CH_3OH, and 13.044 GHz SO observations are listed in Tables 3, and 4 respectively. In the case of 12.2 GHz CH_3OH, absorption was detected only in the pointing positions (108″,0) and (0, −108″); we highlight the absorption spectra in Figure 7. Table 5 lists the line parameters of other transitions of H_2CO, CH_3OH, and NH_3.

We note that McCauley et al. (2011) also report GBT observations of the 1 cm H_2CO line toward NGC 7538 IRS1. At a first glance, the spectrum in their Figure 1 shows a very similar line profile to the one shown in our Figure 1. However, converting their peak T_A^* to flux density (following the flux calibration notes in their Section 3) results in a value lower than ours by a factor of ~0.4 (the same is obtained if we calibrate our data directly to T_A^* in GBTIDL). We argue that the line parameter values reported in this work (Table 5) are more reliable than the values reported by McCauley et al. (2011) in their Table 2 because: 1) as explained in Section 2.2, we observed the NRAO K. Jansky Very Large Array (VLA) flux density calibrator 3C48 to independently check our flux density scale and our measurement agrees within 12% with the expected value[11], 2) the line parameters of the 1 cm H_2CO line

[9] https://irsa.ipac.caltech.edu/data/SPITZER/Enhanced/SEIP/
[10] http://www.aoc.nrao.edu/~vlbacald/ArchIndex.shtml

[11] Note that our observations were conducted years before the 3C48 flare began in 2018; https://science.nrao.edu/facilities/vla/docs/manuals/oss/performance/fdscale.

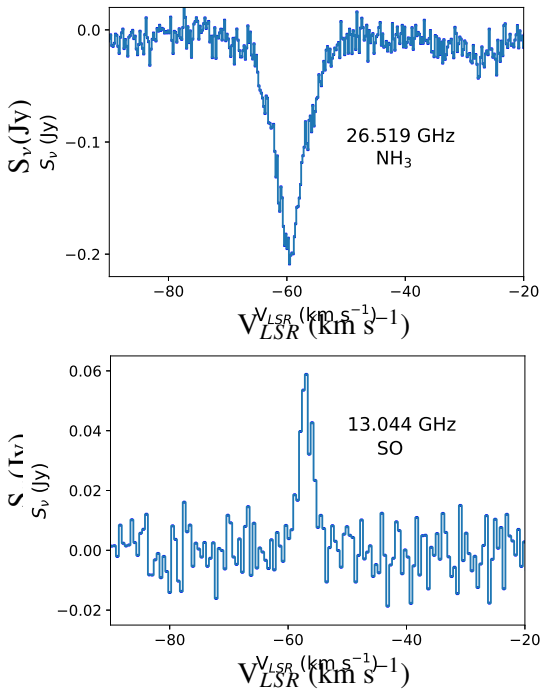

Figure 3. Detection of NH_3 absorption and SO emission in NGC 7538 IRS1. The data shown in the figure are available as Supporting Information.

reported in Table 2 of McCauley et al. (2011) show that the line was fit with two overlapping Gaussians, one absorption and one emission line, but both with approximately the same absolute intensity (0.1 K), which disagrees with the line profile of the 1 cm H_2CO line where the emission clearly has a greater line intensity than the absorption (e.g., Figure 1). By assuming that both emission and absorption features have similar absolute intensities, the linewidths of the overlapping Gaussians reported by McCauley et al. (2011) were significantly broader than what the spectrum suggests.

4 ANALYSIS AND DISCUSSION

Figure 4 shows extended 2 cm H_2CO absorption toward the East, West, and South of NGC 7538 IRS1. The figure also shows 2 cm emission overlapping absorption toward the center of the cross-scan. While it is clear that the absorption is extended, the extent of the emission is not as clear because of the superposition with absorption. In this section we discuss deconvolution of the emission and absorption features to measure the angular size of the 2 cm H_2CO emission, and thus, to disentangle whether the emission is caused by a maser or a (quasi-)thermal mechanism.

4.1 2 cm H_2CO Absorption

As shown in Figure 4, absorption was detected in 11 pointing positions; the two exceptions are the far North positions at (0, 108″) and (0, 54″), where neither emission nor absorption were detected. The absorption is also less prominent toward the West of NGC 7538 IRS1. As also shown in Figure 4, the peak of the cm radio continuum from the extended ionized gas (VLA contours) is located to the North-West of NGC 7538 IRS1 (see also, e.g., Ojha et al. 2004). A larger scale GBT continuum image of the region is reported in Luisi et al. (2016), which shows that the diffused radio continuum emission from the HII region extends beyond a 300″ area, i.e., greater than the field of view of Figure 4.

Based on the line profiles from the unconstrained-fits shown in Figure 5, the pointing positions (108″,0), (54″,0), (−108″,0) and (0,−108″) are the least affected by overlapping absorption and emission lines (see Figure 4). As mentioned above, in order to characterize the emission, we need to reliably deconvolve the absorption from the emission in the central pointing positions. To accomplish this, we have to characterize the absorption profiles toward the pointing positions with significant emission overlap. Comparing the velocities of the H_2CO absorption not affected by emission in the East-West direction, i.e., V_{LSR} (108″, 0) = −54.69(0.38) km s^{-1}, V_{LSR} (54″, 0) = −55.19(0.07) km s^{-1}, V_{LSR} (−108″, 0) = −57.22(0.15) km s^{-1} (see Table 1), we find a smooth velocity gradient across the East-West scan, with redshifted absorption toward the East and blueshifted absorption toward the West. We note that similar velocity gradients are seen at ∼ 1′ scales, e.g., HCO^+ (Figure 7 of Sun & Gao (2009), with the caveat that the HCO^+ (1-0) map is centered 1.3′ South of IRS1; see also Sandell et al. 2012), CO (Qiu et al. 2011, Sandell et al. 2012), CS (Kameya et al. 1986), although see the complex NH_3 velocity structure reported by Zheng et al. (2001).

As a way to better constrain the line parameters of the absorption, we spatially interpolated the peak absorption velocity in the central pointing positions, and fixed the value of the peak absorption in new Gaussian fits of the combined emission+absorption profiles (East-West spectra highlighted in black in Figure 5, left column). As a clear H_2CO absorption profile was not detected toward the North pointing positions, we used the interpolated H_2CO absorption velocity toward the central pointing position (0,0) and the absorption velocity at (0,−108″), i.e., −57.27(0.09) km s^{-1} (see Table 1) to interpolate (and extrapolate in the case of the (0,27″) pointing) the H_2CO peak absorption velocities in the North-South direction, and used them as fixed parameters to fit the emission spectra (Figure 5, right column). The Gaussian fits of the emission components obtained by constraining the peak absorption velocities are shown with orange solid lines in Figure 5; the line parameters are listed in Table 2. Inspection of the fits in Figure 5 shows that constraining peak absorption velocities results in detection of a weak emission line toward the (0,27″) position, and reasonable fits for all but the (0,−54″) pointing position, where the line profile is fit by two overlapping lines, an emission and absorption line of similar absolute peak intensities. Both the free and constrained Gaussian fits show that we cannot reliably measure the line parameters of the emission line toward (0,−54″), as demonstrated by the large peak flux density uncertainty for this pointing position (Table 2). The (0,−54″) pointing includes NGC 7538S, which shows a complex multi-peak emission profile in H_2CO rotational transitions (e.g., Sandell & Wright 2010), which likely contributes to the observed complex line profile.

A graphical view of the absorption line parameters obtained from the unconstrained (Table 1) and constrained (Table 2) fits is shown in Figure 9. While some differences between the two fits are evident (e.g., line velocities), both sets of absorption line parameters show a consistent description of the molecular cloud traced by 2 cm H_2CO. For instance, the line parameters obtained from both methods show that the linewidth of the absorption in the East-West scan is greater toward the central pointing position where active star formation is taking place (e.g., Moscadelli & Goddi 2014).

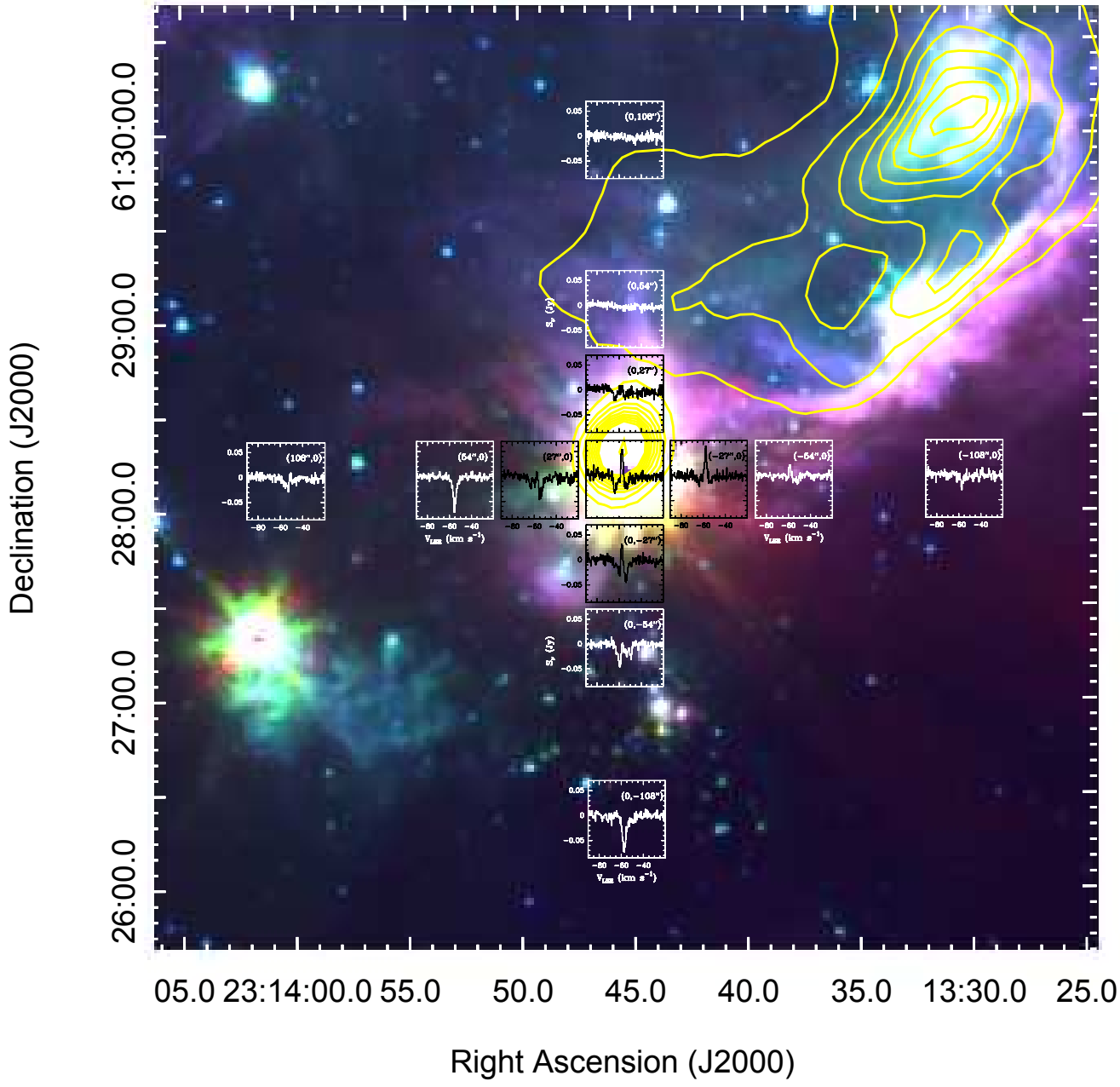

Figure 4. Cross-scan map of 2 cm H_2CO obtained with the GBT. The spectra are superimposed with a three-color (3.6 μm, 4.5 μm and 5.8 μm) Spitzer/IRAC image of NGC 7538. The central position of the cross scan map is R.A=$23^h13^m45.36^s$ and Dec=+61°28′10.45″(J2000). Each spectrum box is 25″× 25″ in size (high-resolution images of the spectra are shown in Figure 5). The HPBW of the GBT at 2 cm is 52″, thus, the offsets from the central position are half-beam, full-beam, and two-beam spacing in the E-W and N-S directions. The yellow contours show 6 cm VLA continuum from the NRAO image archive. The contour levels start at 39 mJy beam^{-1} and continuing to 1104 mJy beam^{-1} (peak intensity) in steps of 59 mJy beam^{-1} × (1, 2, 3, 4, 5, 6, 7, 8, 17, 18). Note that four pointing positions [(−108″,0),(0,−108″),(54″,0),(108″,0)] do not show strong evidence of overlapping emission and absorption lines.

The greater linewidth could be due to greater turbulence at the star formation site and/or to the molecular outflow in NGC 7538 IRS1 (e.g., Wright et al. 2014).

4.2 Line Parameters and Angular Size of the 2 cm H_2CO Emission Region

As discussed below, our observations show that the 2 cm H_2CO emission has a much wider spatial distribution than the 6 cm H_2CO masers imaged by Hoffman et al. (2003) and the multiple disk system around massive YSOs in the central region of IRS1 as shown by VLBI observations (Moscadelli & Goddi 2014). Table 2 shows the line parameters of the emission lines after fixing the peak velocity of the absorption in each pointing position. The LSR velocity of the emission line at the center position from the constrained fit is −57.3(0.1) km s^{-1}, which agrees within the errors with the velocity of −57.34(0.07) km s^{-1} obtained from the unconstrained fit (Table 1). This peak velocity also agrees with the systemic veloc-

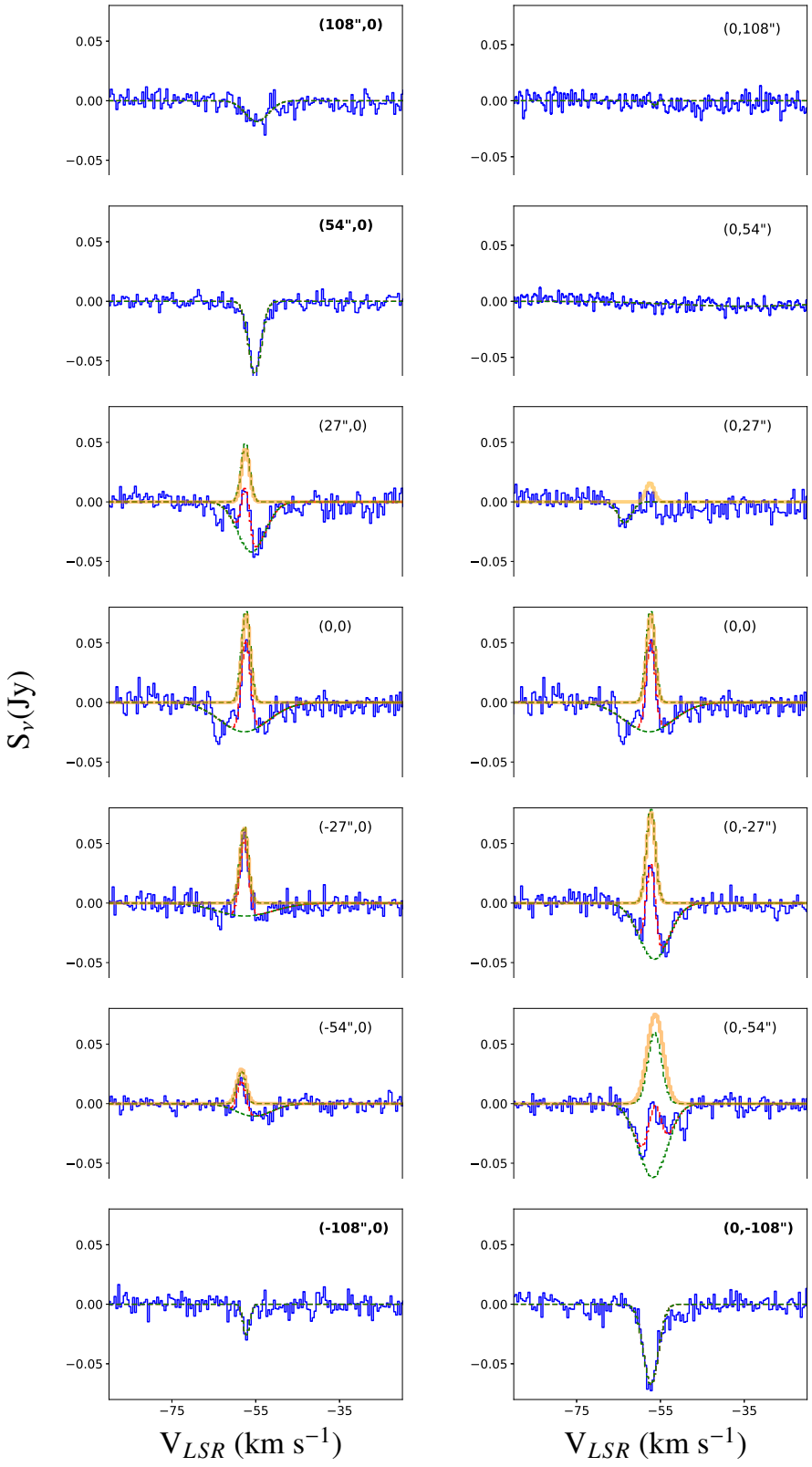

Figure 5. Spectra of 2 cm H_2CO emission and absorption toward NGC 7538. Gaussian fits are included as dashed lines (green curves show individual components, red curves show the combined fit when more than one component was fit). The East-West spectra are shown in the left column, the North-South pointings are shown in the right column. Note that the same central pointing spectrum is shown in both the left and right columns. The highlighted spectra (bold coordinates) were used to interpolate the H_2CO absorption velocities (see Section 4.1 and Figure 4). Thick solid (orange) lines are Gaussian fits of the emission lines after constraining the peak absorption velocities (see Section 4.1). The data shown in the figure are available as Supporting Information.

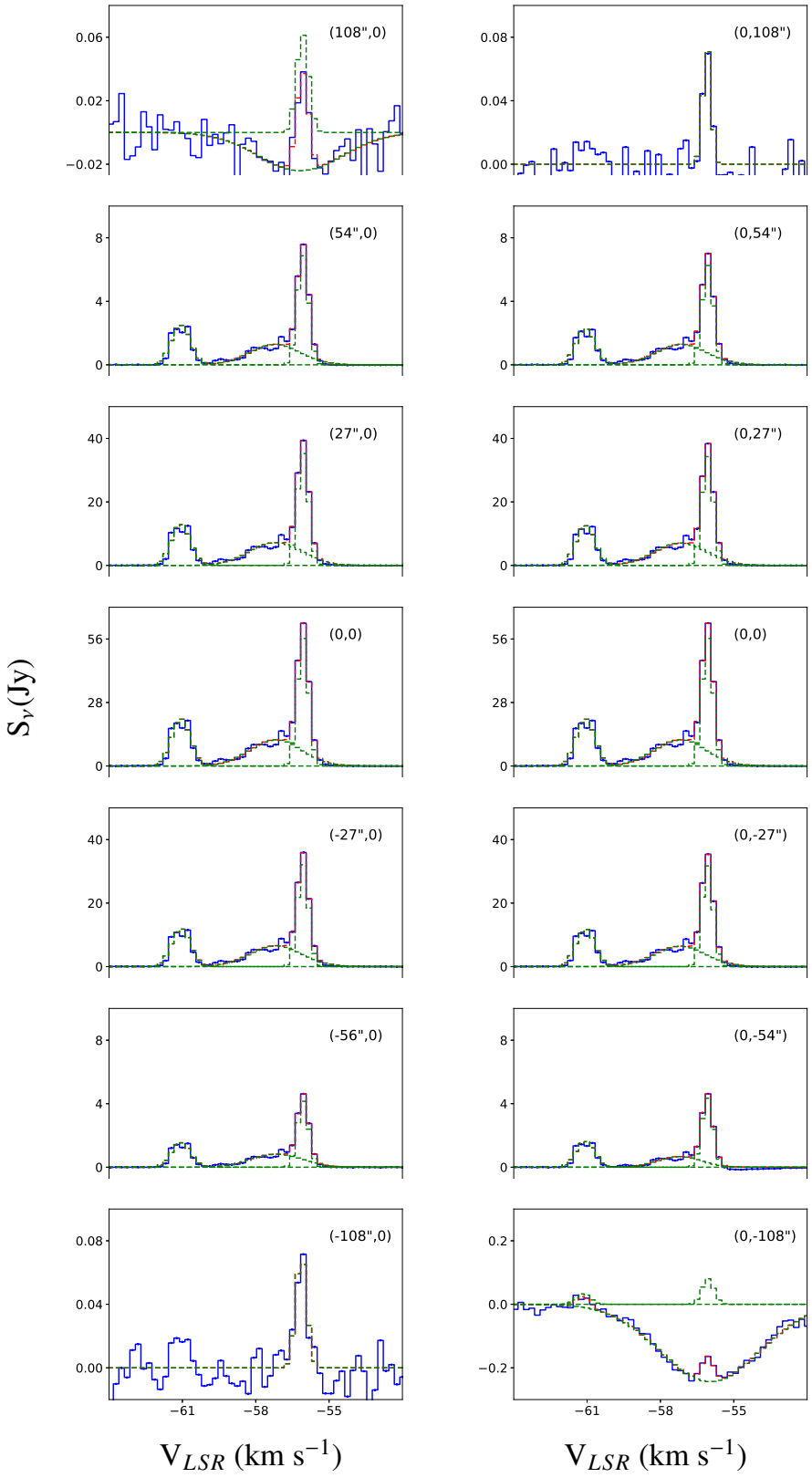

Figure 6. Same as Figure 5 but for 12.2 GHz CH_3OH. We show the same velocity range in all panels for consistency; however, the velocity range was optimized for emission and not for the (108″,0) and (0,−108″) pointings that show significant absorption. The two absorption spectra are shown with a larger velocity range in Figure 7. The data shown in the figure are available as Supporting Information.

Table 1. Line parameters of 2 cm H_2CO observations.

Position (ΔRA, ΔDec)	S_ν (Jy)	RMS (Jy)	V_{LSR} (km s^{-1})	Width (km s^{-1})	$\int S_\nu dv$ (Jy km s^{-1})
NGC7538 IRS1	0.077(0.005)	0.006	−57.34(0.07)	2.5(0.2)	0.21(0.03)
	−0.025(0.003)	0.006	−57.75(0.52)	13.6(1.5)	−0.36(0.09)
(108″,0)	−0.018(0.002)	0.007	−54.69(0.38)	6.5(0.9)	−0.12(0.03)
(54″,0)	−0.061(0.002)	0.004	−55.19(0.07)	3.6(0.2)	−0.23(0.02)
(27″,0)	0.049(0.006)	0.008	−57.47(0.12)	2.4(0.4)	0.13(0.04)
	−0.042(0.006)	0.008	−56.01(0.32)	7.7(0.6)	−0.34(0.08)
(−27″,0)	0.064(0.004)	0.006	−57.76(0.07)	2.4(0.2)	0.17(0.02)
	−0.011(0.002)	0.006	−57.50(1.10)	15.8(3.0)	−0.18(0.07)
(−54″,0)	0.027(0.003)	0.004	−58.39(0.12)	2.4(0.3)	0.07(0.02)
	−0.011(0.002)	0.004	−55.46(0.86)	10.0(1.5)	−0.11(0.04)
(−108″,0)	−0.026(0.004)	0.006	−57.22(0.15)	1.9(0.4)	−0.05(0.02)
(0,108″)	...	0.006	...	...	...
(0,54″)	...	0.005	...	...	...
(0,27″)	−0.018(0.004)	0.007	−63.51(0.38)	3.7(0.9)	−0.07(0.03)
(0,−27″)	0.079(0.006)	0.006	−57.29(0.06)	2.6(0.2)	0.21(0.03)
	−0.047(0.006)	0.006	−56.48(0.21)	8.4(0.6)	−0.42(0.08)
(0,−54″)	0.060(0.019)	0.005	−56.37(0.14)	3.9(0.7)	0.25(0.12)
	−0.062(0.019)	0.005	−56.85(0.22)	8.0(0.9)	−0.53(0.22)
(0,−108″)	−0.067(0.003)	0.006	−57.27(0.09)	4.2(0.2)	−0.30(0.03)

Line parameters obtained from Gaussian fits, 1σ statistical errors from the fit are reported in parenthesis. The spectra were smoothed to a channel width of 0.442 km s^{-1}.

Table 2. Line parameters of 2 cm H_2CO for pointing positions that were fit after constraining the absorption velocities.

Position (ΔRA, ΔDec)	S_ν (Jy)	RMS (Jy)	V_{LSR} (km s^{-1})	Width (km s^{-1})	$\int S_\nu dv$ (Jy km s^{-1})
NGC7538 IRS1	0.074(0.005)	0.006	−57.3(0.1)	2.3(0.2)	0.18(0.03)
	−0.020(0.003)	0.006	−55.91*	15.8(1.8)	−0.35(0.09)
(27″,0)	0.045(0.005)	0.008	−57.43(0.12)	2.2(0.3)	0.10(0.03)
	−0.039(0.004)	0.008	−55.59*	7.7(0.6)	−0.32(0.05)
(−27″,0)	0.063(0.004)	0.006	−57.75(0.07)	2.3(0.2)	0.16(0.02)
	−0.010(0.002)	0.006	−56.24*	17.7(3.3)	−0.18(0.07)
(−54″,0)	0.029(0.003)	0.004	−58.39(0.12)	2.6(0.3)	0.08(0.02)
	−0.012(0.002)	0.004	−56.56*	10.0(1.5)	−0.12(0.04)
(0,27″)	0.016(0.005)	0.007	−57.49(0.30)	2.3(0.8)	0.04(0.03)
	−0.011(0.002)	0.007	−55.57*	19.7(3.3)	−0.24(0.08)
(0,−27″)	0.076(0.005)	0.006	−57.28(0.06)	2.5(0.2)	0.20(0.03)
	−0.044(0.004)	0.006	−56.25*	8.6(0.6)	−0.41(0.07)
(0,−54″)	0.075(0.032)	0.005	−56.24(0.15)	4.5(0.7)	0.36(0.21)
	−0.078(0.033)	0.005	−56.60*	7.7(0.9)	−0.64(0.34)

* Fixed parameter in the fit, thus, no uncertainty reported. All other uncertainties are 1σ statistical errors from the fit.

ity from $C^{17}O$ and $C^{34}S$ transitions reported by Van der Tak et al. (2000).

Figure 10 shows the line parameters from the free (Table 1) and constrained (Table 2) fits for the emission line. As demonstrated in the figure, the line parameters of the emission line are not greatly modified by constraining the absorption velocities. This indicates that the line parameters of the emission are reliably measured, with the exception of the (0,−54″) pointing. We find that the linewidth is approximately uniform across the four East-West pointing positions, which indicates that the emission line is tracing a relatively uniform turbulent environment. We also found an East-West velocity gradient (Figure 10). At smaller scales than our cross-scan (∼ 40″), Wright et al. (2014) find a CO outflow centered on NGC 7538 IRS1 that is red-shifted toward the South-East and blue-shifted toward the North-West; a complete half-beam spacing mapping of the 2 cm H_2CO emission in the region is necessary to further investigate the nature of the observed velocity gradient and its possible connection with the outflow in NGC 7538 IRS1, rotation or infall.

As shown in the upper panels of Figure 10, the 2 cm H_2CO emission peaks near the center pointing position, i.e., (0,0). In Figure 11 we show the emission peak flux density values from Table 2 for the East-West and North-South scans (Figure 4) fitted with Gaussian distributions. As the figure demonstrates, a Gaussian function reproduces reasonably well the East-West distribution of H_2CO emission. The FWHM of the 2 cm H_2CO spatial distribution is 72″± 6″ in the East-West direction. Due to the large uncertainty in the peak emission at (0,−54″), the angular size from the North-South scan is not well-constrained. The fit of the data points (without relative weights due to different error bars) results in a FWHM of 81″± 12″ in the North-South direction (solid blue fit, Figure 11), however, when relative weights are included, the FWHM is 54″± 6″ (blue dotted line, Figure 11). Assuming a Gaussian GBT beam of 52″± 1″, the deconvolved angular size (at half maximum; assuming Gaussian distributions) of the 2 cm H_2CO emission is 50″± 8″ in the East-West direction. In the North-South, we obtained a FWHM of 62″± 16″ without data weights, however, the large un-

Table 3. Line parameters of 12.2 GHz CH_3OH observations.

Position (ΔRA, ΔDec)	S_ν (Jy)	RMS (Jy)	V_{LSR} (km s^{-1})	Width (km s^{-1})	$\int S_\nu dv$ (Jy km s^{-1})
NGC7538 IRS1	56.45(0.64)	0.01	−56.071(0.003)	0.55(0.01)	32.87(0.83)
	11.57(0.28)	0.01	−57.17(0.04)	2.51(0.08)	30.91(1.66)
	20.86(0.42)	0.01	−61.07(0.01)	0.92(0.02)	20.35(0.88)
(108″,0)	0.06(0.01)	0.01	−56.09(0.04)	0.58(0.12)	0.04(0.01)
	−0.02(0.01)	0.01	−56.18(0.30)	4.09(0.81)	−0.11(0.04)
(54″,0)	6.9(0.1)	0.01	−56.073(0.003)	0.55(0.01)	4.01(0.10)
	1.29(0.03)	0.01	−57.20(0.05)	2.46(0.09)	3.38(0.21)
	2.52(0.05)	0.01	−61.07(0.01)	0.91(0.02)	2.45(0.11)
(27″,0)	35.4(0.4)	0.01	−56.072(0.003)	0.55(0.01)	20.58(0.52)
	7.17(0.17)	0.01	−57.18(0.04)	2.51(0.08)	19.12(1.03)
	12.99(0.26)	0.01	−61.07(0.01)	0.92(0.02)	12.66(0.54)
(−27″,0)	32.20(0.40)	0.01	−56.070(0.003)	0.55(0.01)	18.75(0.48)
	6.59(0.16)	0.01	−57.16(0.04)	2.51(0.08)	17.57(0.95)
	11.93(0.24)	0.01	−61.07(0.01)	0.92(0.02)	11.6(0.5)
(−54″,0)	4.17(0.05)	0.01	−56.069(0.003)	0.55(0.01)	2.42(0.06)
	0.83(0.02)	0.01	−57.15(0.04)	2.43(0.08)	2.14(0.12)
	1.56(0.03)	0.01	−61.07(0.01)	0.91(0.02)	1.51(0.07)
(−108″,0)	0.07(0.01)	0.01	−56.14(0.03)	0.53(0.08)	0.04(0.01)
(0,108″)	0.07(0.01)	0.01	−56.10(0.03)	0.41(0.07)	0.03(0.01)
(0,54″)	6.26(0.07)	0.01	−56.062(0.003)	0.55(0.01)	3.64(0.10)
	1.30(0.03)	0.01	−57.14(0.04)	2.48(0.07)	3.42(0.18)
	2.27(0.05)	0.01	−61.06(0.01)	0.92(0.02)	2.21(0.10)
(0,27″)	34.4(0.4)	0.01	−56.067(0.003)	0.55(0.01)	20.05(0.51)
	7.05(0.17)	0.01	−57.16(0.04)	2.5(0.1)	18.8(1.0)
	12.59(0.25)	0.01	−61.06(0.01)	0.92(0.02)	12.27(0.53)
(0,−27″)	31.87(0.37)	0.01	−56.074(0.003)	0.55(0.01)	18.54(0.48)
	6.44(0.16)	0.01	−57.18(0.04)	2.48(0.08)	17.02(0.95)
	11.85(0.24)	0.01	−61.07(0.01)	0.92(0.02)	11.6(0.5)
(0,−54″)	4.38(0.07)	0.01	−56.080(0.003)	0.55(0.01)	2.54(0.08)
	0.67(0.03)	0.01	−57.23(0.07)	2.06(0.14)	1.47(0.15)
	1.63(0.04)	0.01	−61.08(0.01)	0.90(0.02)	1.57(0.08)
(0,−108″)	−0.24(0.01)	0.01	−55.97(0.04)	4.8(0.1)	−1.25(0.05)
	0.08(0.01)	0.01	−56.06(0.04)	0.6(0.1)	0.05(0.02)
	0.03(0.01)	0.01	−61.2(0.1)	0.68(0.23)	0.024(0.015)

Line parameters obtained from Gaussian fits, 1 σ statistical errors from the fit are reported in parenthesis. The spectra were smoothed to a channel width of 0.225 km s^{-1}.

Table 4. Line parameters of 13.044 GHz SO observations.

Position (ΔRA, ΔDec)	S_ν (Jy)	RMS (Jy)	V_{LSR} (km s^{-1})	Width (km s^{-1})	$\int S_\nu dv$ (Jy km s^{-1})
NGC7538 IRS1	0.052(0.004)	0.007	−56.99(0.18)	2.8(0.3)	0.16(0.03)
(108″,0)	...	0.008	...	...	...
(54″,0)	0.052(0.003)	0.005	−56.86(0.07)	2.6(0.7)	0.15(0.02)
(27″,0)	0.055(0.005)	0.007	−57.09(0.11)	2.7(0.3)	0.16(0.03)
(−27″,0)	0.028(0.004)	0.007	−57.22(0.23)	3.04(0.54)	0.09(0.03)
(−54″,0)	0.008(0.002)	0.005	−57.5(0.7)	6.49(1.66)	0.06(0.03)
(−108″,0)	0.011(0.005)	0.006	−56.58(0.41)	1.84(0.96)	0.02(0.02)
(0,108″)	...	0.008	...	...	...
(0,54″)	...	0.005	...	...	...
(0,27″)	0.018(0.004)	0.005	−56.62(0.29)	2.49(0.69)	0.05(0.03)
(0,−27″)	0.067(0.004)	0.008	−57.25(0.10)	3.39(0.23)	0.24(0.03)
(0,−54″)	0.075(0.002)	0.004	−56.5(0.1)	4.45(0.16)	0.36(0.02)
(0,−108″)	0.057(0.003)	0.007	−56.02(0.11)	3.72(0.25)	0.23(0.03)

Line parameters obtained from Gaussian fits, 1 σ statistical errors from the fit are reported in parenthesis. The spectra were smoothed to a channel width of 0.491 km s^{-1}.

certainty in the (0,−54″) emission flux density precludes us from obtaining a reliable source size in the North-South direction. Nevertheless, our data reliably show that the 2 cm H_2CO emission region is extended (∼ 50″) at least in the East-West direction. A complete (half-beam spacing) map of the 2 cm H_2CO line, instead of a cross-scan, is needed to better characterize the absorption and thus, better deconvolve the emission from the absorption. As pointed out by McCauley et al. (2011), mapping is necessary to obtain reliable source sizes for densitometry studies using H_2CO K-doublets.

Our simultaneous cross-scan observations of 12.2 GHz

Table 5. Line parameters of the other transitions.

Spectral Line	S_ν (Jy)	RMS (Jy)	V_{LSR} (km s^{-1})	Width (km s^{-1})	$\int S_\nu dv$ (Jy km s^{-1})
1 cm H_2CO	0.099(0.003)	0.007	−56.68(0.04)	2.6(0.1)	0.27(0.02)
	−0.034(0.004)	0.007	−64.3(0.1)	2.04(0.25)	−0.08(0.02)
6 cm H_2CO	0.443(0.006)	0.014	−60.12(0.01)	0.84(0.02)	0.40(0.01)
	1.310(0.006)	0.014	−57.905(0.002)	0.94(0.01)	1.32(0.01)
	−0.218(0.002)	0.014	−55.95(0.05)	6.65(0.09)	−1.55(0.04)
26.847 GHz CH_3OH	−0.156(0.002)	0.009	−59.58(0.04)	5.8(0.1)	−0.97(0.03)
28.316 GHz CH_3OH	−0.101(0.003)	0.008	−59.7(0.1)	4.1(0.1)	−0.44(0.03)
28.970 GHz CH_3OH	0.128(0.006)	0.007	−59.28(0.05)	1.8(0.1)	0.25(0.03)
	0.264(0.005)	0.007	−56.26(0.02)	2.17(0.06)	0.61(0.03)
26.518 GHz NH_3	−0.179(0.003)	0.009	−59.49(0.07)	6.91(0.16)	−1.32(0.06)

Line parameters obtained from Gaussian fits, 1σ statistical errors from the fit are reported in parenthesis. All spectra were smoothed to a channel width of 0.2 km s^{-1}, with exception of the 6 cm H_2CO line (0.047 km s^{-1} channel width) to fit the narrow masers.

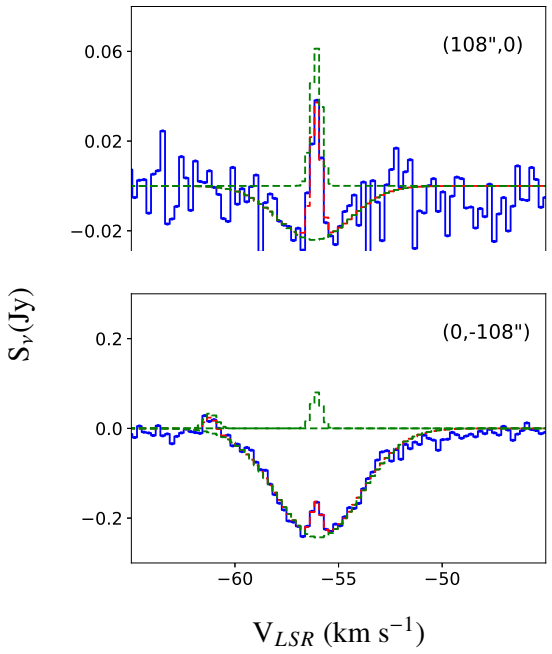

Figure 7. Spectra and Gaussian fits for the two pointing positions with prominent 12.2 GHz CH_3OH absorption as shown in Figure 6, i.e., (108″,0) and (0, −108″). The data shown in the figure are available as Supporting Information.

CH_3OH and 13.044 GHz SO allow us to conduct an independent test of the reliability of the H_2CO angular size determination. Figures 12 and 13 are as Figure 11 but for the 12.2 GHz CH_3OH and 13.044 GHz SO cross-scans, respectively. In the case of 12.2 GHz CH_3OH, it is well-known that the emission is caused by compact high-brightness temperature masers located within 1″ of NGC 7538 IRS1, e.g, Minier et al. (2002). We note that our 12.2 GHz CH_3OH spectrum of NGC 7538 IRS1 (Figure 6) shows the same line profile as the VLBI spectrum shown in figure 2 of Minier et al. (2002), albeit with a different flux density, which is not surprising as multiple maser species are known to be variable in NGC 7538 IRS1, e.g., Andreev et al. (2017). Given the compact distribution of 12.2 GHz CH_3OH masers in the region, we expect our cross-scan to result in an unresolved source size. The Gaussian spatial fits of the CH_3OH data give a FWHM of 60″± 1″ (average of the East-West and North-South FWHM; Figure 12). Given the GBT beam of 62″± 1″ at 12.2 GHz, this implies an unresolved source, i.e., the masers are unresolved, as expected. The case of 13.044 GHz SO is the opposite extreme: as shown in Figure 13 the emission is extended, with a deconvolved size of 75″ (East-West) and 114″ (North-South), and the emission is not centered at NGC 7538 IRS1. These CH_3OH and SO tests validate our deconvolution strategy.

We conclude that the 2 cm H_2CO emission in NGC 7538 IRS1 is resolved; it is tracing a molecular core of ∼50″ FWHM size (∼ 0.7 pc) in the East-West direction, and possibly narrower in the North-South direction. This physical size is more extended than the hypercompact HII region near NGC 7538 IRS1 (Gaume et al. 1995) and than the molecular core assumed by McCauley et al. (2011), i.e., 16″; while it is similar to the size of the millimeter and sub-millimeter dust core reported by Sandell & Sievers (2004) (e.g., see their figure 3), and more compact than the NH_3 (1,1) molecular cloud imaged by Keown et al. (2019). The physical size we measured is similar to the extent of the 2 cm H_2CO emission filament-like structure in OMC-1 (Bastien et al. 1985). In summary, our observations clearly show that the 2 cm H_2CO emission does not originate from the sub-arcsecond 6 cm maser region (Hoffman et al. 2003), but from an extended molecular cloud.

4.3 Nature of the 2 cm H_2CO Emission

Based on the angular size of the 2 cm H_2CO emission region discussed above, we obtain a peak brightness temperature of 0.33 K (assuming a symmetric Gaussian distribution of FWHM equal to the East-West major axis), which is consistent with optically thin thermal emission.

The non-detection of 2 cm H_2CO emission by Hoffman et al. (2003) is consistent with the angular size and brightness temperature values reported here. Hoffman et al. (2003) employed the VLA CnB configuration for which the shortest baselines were 65 m, corresponding to a largest angular scale of ≈ 60″at 2 cm. The 2 cm emission that we describe here would have been significantly filtered out by the interferometer. Moreover, the RMS brightness temperature of the 2 cm H_2CO VLA observations reported by Hoffman et al. (2003) is ∼ 10 K, which is much greater than the peak brightness temperature we obtained from the GBT observations (0.33 K), thus, the extended region would have been resolved out.

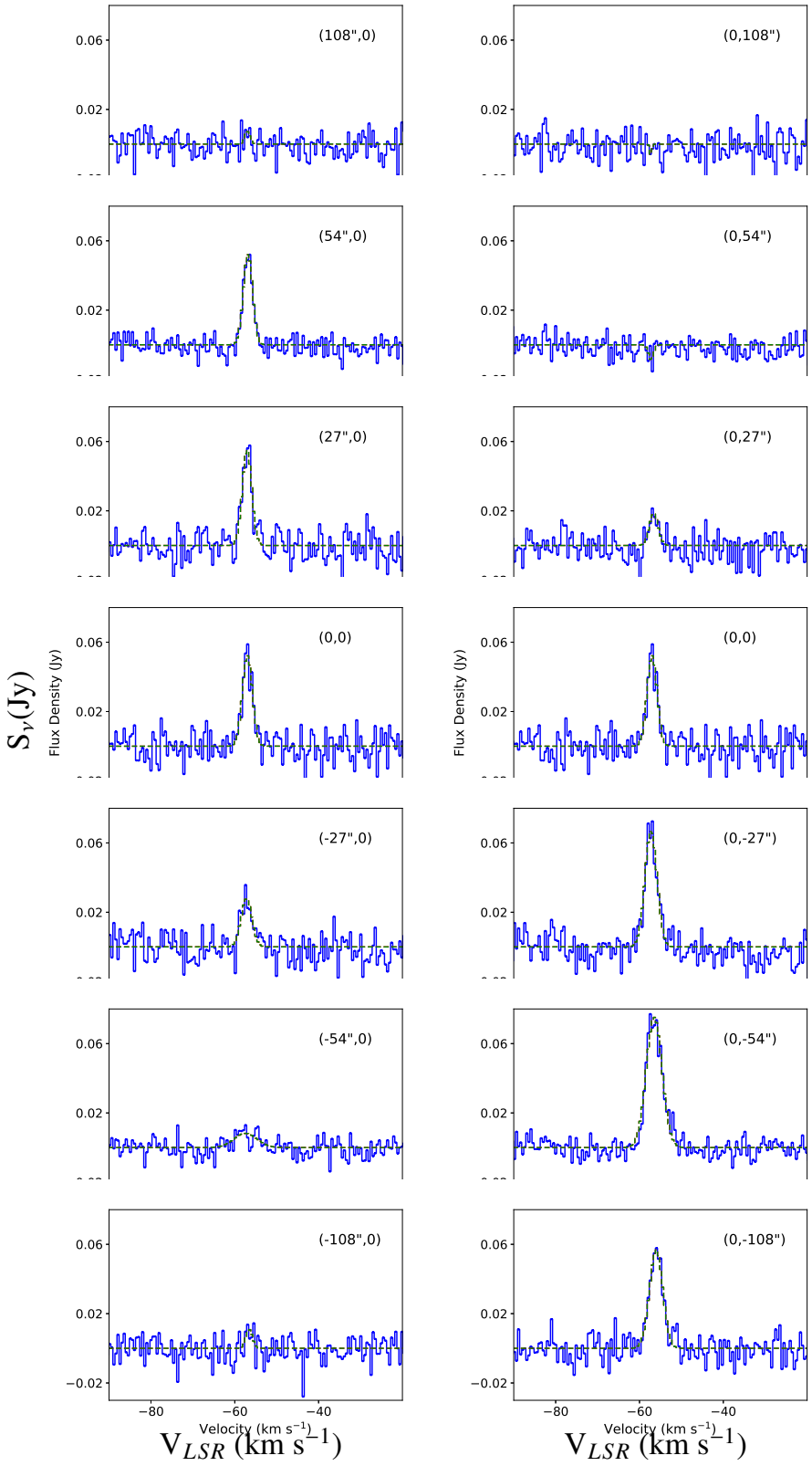

Figure 8. Same as Figure 5 but for 13 GHz SO. The data shown in the figure are available as Supporting Information.

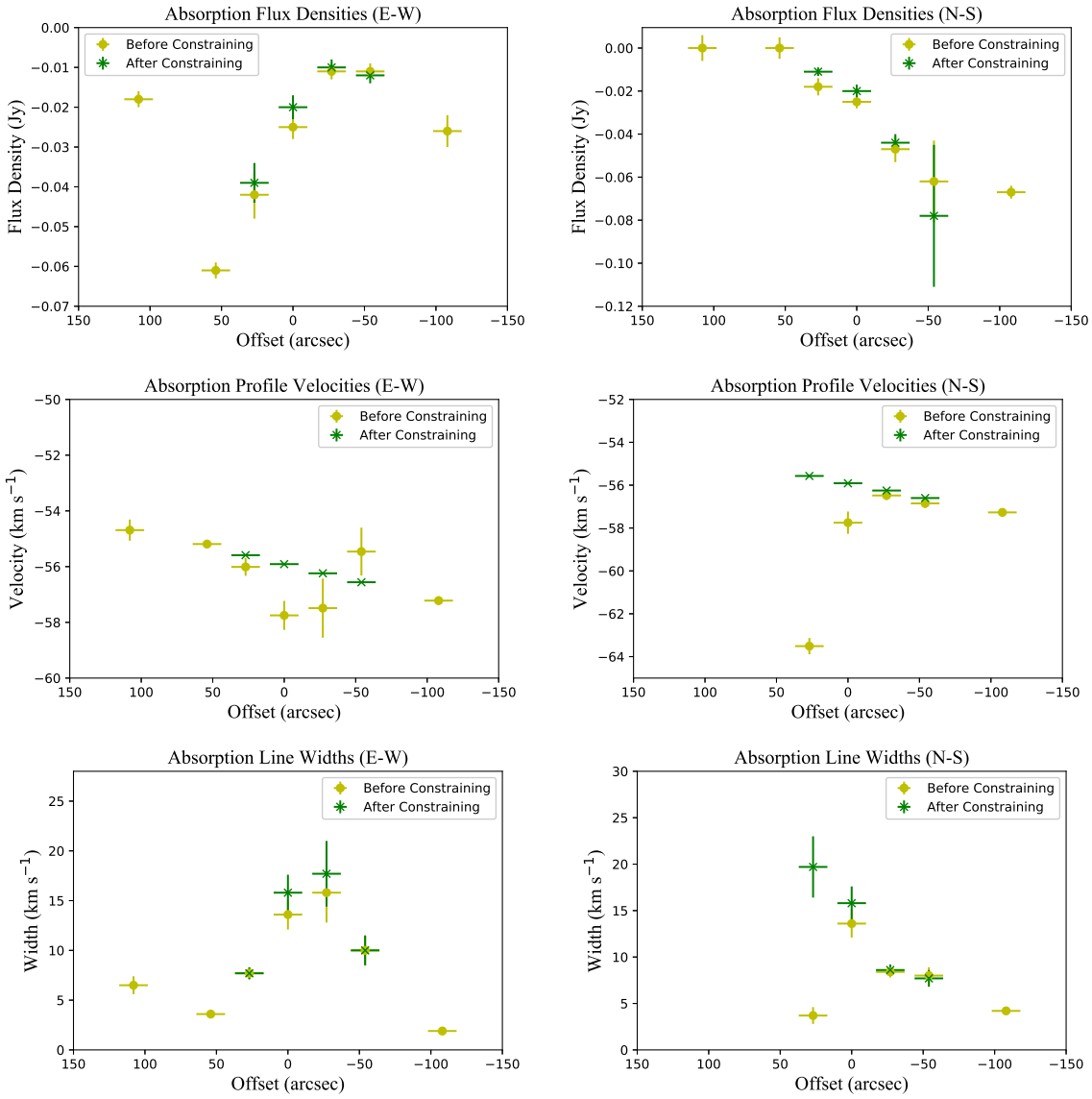

Figure 9. Line parameters of 2 cm H_2CO absorption (flux density, velocity and linewidth) from the cross-scan observations of NGC 7538 IRS1. Left and right panels show the East-West and North-South scans, respectively. Two different symbols are used to show the line parameters from the unconstrained (Table 1) and constrained Gaussian fits (Table 2).

As shown in Figure 1 (see also Table 5), we detected 1 cm H_2CO emission in NGC 7538 IRS1. Given the similar line profiles of the 2 cm and 1 cm lines, it is likely that the 1 cm transition is also due to thermal emission (see profiles of the 6 cm H_2CO masers with respect to the 1 cm and 2 cm lines in Figure 1). Assuming LTE excitation of the 1 and 2 cm lines and optically thin emission, we can estimate the excitation temperature of the gas by using the ratio of population levels (e.g., see equations A5 and A11 in Araya et al. 2005). We estimate an LTE excitation temperature of ~ 20 K, which is similar to the value obtained for OMC-1 (Bastien et al. 1985).

To further explore the physical conditions that can lead to thermal emission of the 2 cm and 1 cm lines, without detectable emission of a thermal line in the 6 cm transition, we modeled our multi-transition data using RADEX, which is a one dimensional non-LTE radiative transfer code developed by Van der Tak et al. (2007). We explored a range of densities between $n_{H_2} = 10^3$ to 10^8 cm^{-3} (with steps of 0.1 in $\log_{10}(n(H_2))$, ortho-H_2CO column densities (N_{o-H_2CO}) between 10^{13} to 10^{15} cm^{-2} (with 10 steps per decade, and finer steps when converging to the final solution), kinetic temperatures between 10 to 500 K (in steps of 10 K), and assumed a simple characterization of the background radio continuum consisting of Cosmic Microwave Background and free-free emission from Luisi et al. (2016) with a turnover frequency near 8 GHz (e.g., Akabane et al. 1991). Refining the model would require mapping the molecular lines and the background radio continuum at the frequencies of interest to determine the appropriate beam-filling factors.

Figure 14 shows the results of the model for the three K-doublet

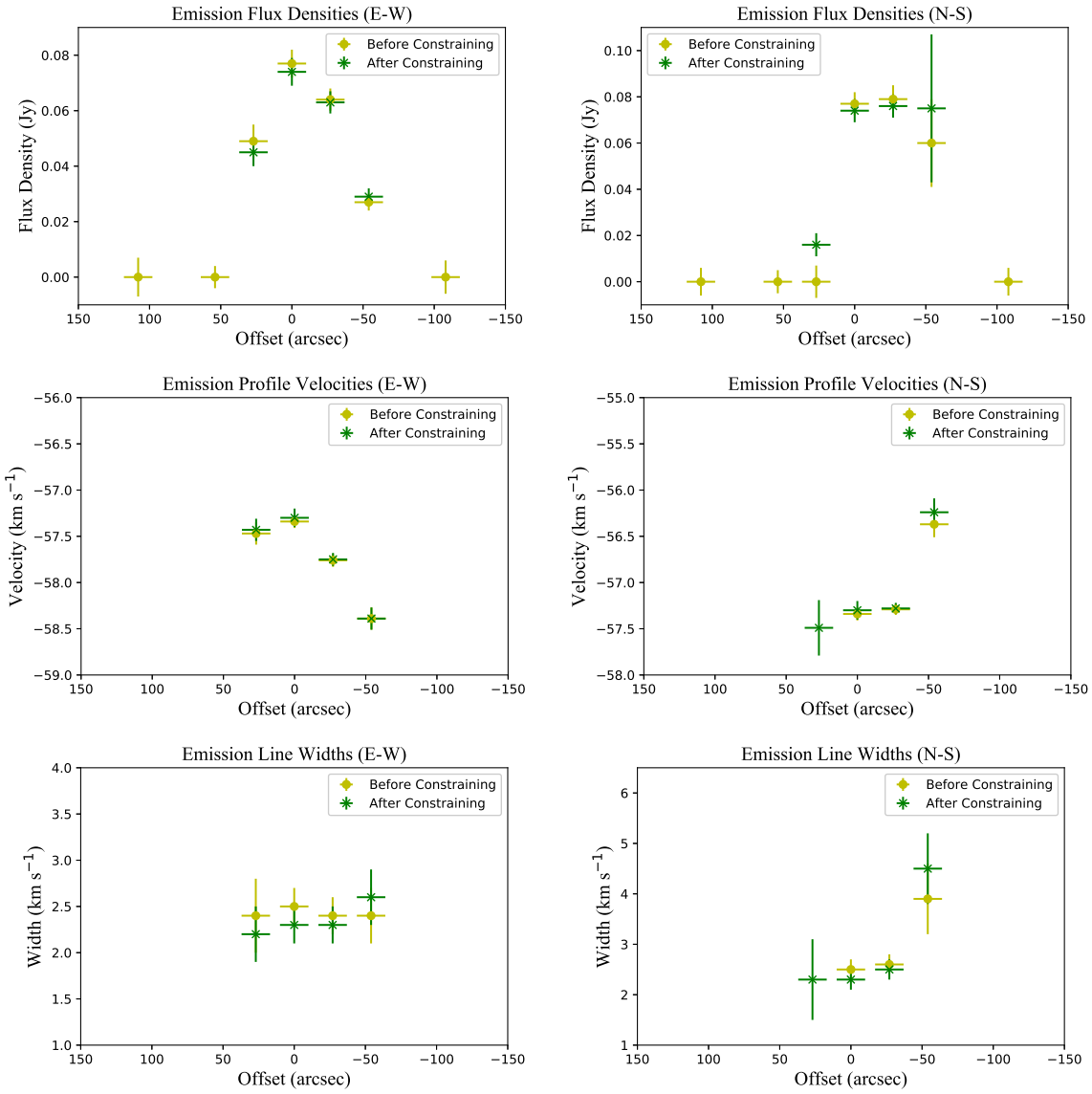

Figure 10. As in Figure 9 but for the emission line. Emission was detected in only the central 4 pointing positions in the East-West scan, and in 4 positions in the North-South scan (see also Figure 4).

transitions included in this work as a function of molecular density at $T_K = 40$ K and $N_{o-H_2CO} = 1.5 \times 10^{14}$ cm^{-2}. We show with a solid line (red), dot-dashed line (green), and dotted line (blue) the predicted flux densities for the 1 cm, 2 cm, and 6 cm H_2CO lines, respectively. With parallel horizontal lines (same line style patterns and colours as above), we show the range of peak flux densities based on our observations. For the 2 cm and 1 cm H_2CO transitions, the range is given by the uncertainties listed in Tables 2 and 5. In the case of the 6 cm H_2CO line (Figure 1), the absorption must be caused by the extended molecular cloud also traced by 2 cm absorption (Figure 4), while the emission lines are caused by very compact masers, e.g., Hoffman et al. (2003). We inspected the 6 cm H_2CO line profile, and concluded that a line asymmetry due to the material traced by 2 cm and 1 cm H_2CO emission is undetectable at a level of ±60 mJy, which is the range shown with horizontal dotted lines (blue) in Figure 14. We find that a gas density of $\sim 10^{5.7}$ cm^{-3} (vertical dashed line in Figure 14) is consistent with our detection of 2 cm and 1 cm H_2CO emission and non-detection of 6 cm thermal emission. This density is similar to the density obtained from the 1 cm and 48 GHz H_2CO lines ($n_{H_2} = 10^{5.78}$ cm^{-3}) by McCauley et al. (2011). We note that McCauley et al. (2011) assumed a source size of 16″, while our cross scan shows that the region traced by 2 cm H_2CO emission is significantly more extended (Section 4.2).

The ortho-H_2CO column density of our model (1.5×10^{14} cm^{-2}) is similar to the value reported by McCauley et al. (2011) ($N_{o-H2CO}/\Delta v = 10^{13.75}$ cm^{-2}(km s^{-1})$^{-1}$, see their Table 4), although the temperature in our model is lower than what they assumed (40 K vs 220 K). We find this temperature difference reasonable because the 2 cm H_2CO emission likely traces a more extended region than that seen at the higher energy 48 GHz H_2CO

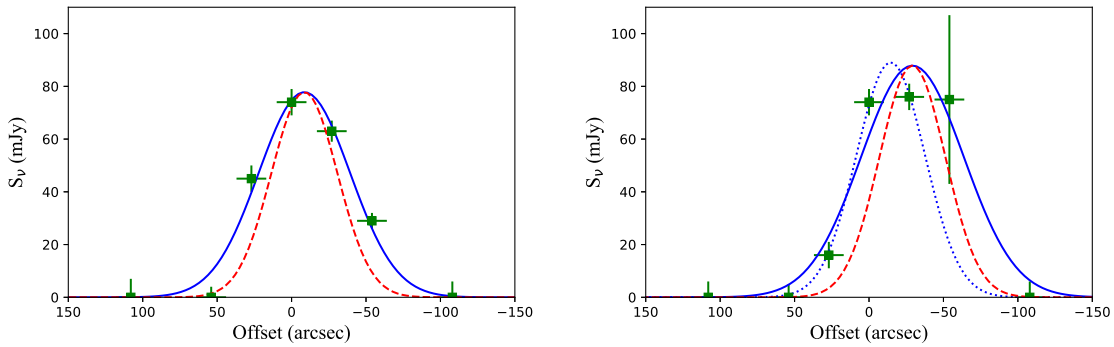

Figure 11. Peak flux density distribution (East-West, left; North-South, right) of 2 cm H_2CO emission (Table 2). Continuous (blue) lines show Gaussian fits of the spatial distribution. In the right panel, we also show the Gaussian fit including relative weights due to different error bars (dotted blue line). Dashed lines in both panels show the beam pattern of the telescope centered at the peak position.

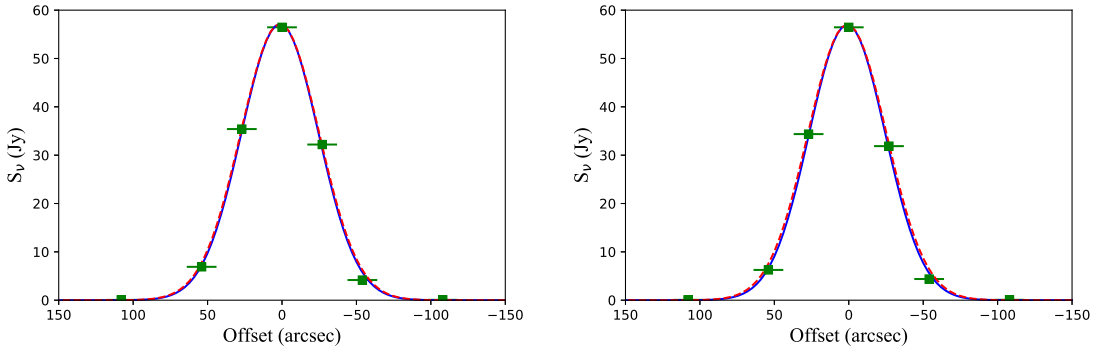

Figure 12. Same as Figure 11 but for the main peak of the 12.2 GHz CH_3OH emission (Table 3). The FWHM of the spatial distribution matches the HPBW of the telescope, i.e., the maser is unresolved.

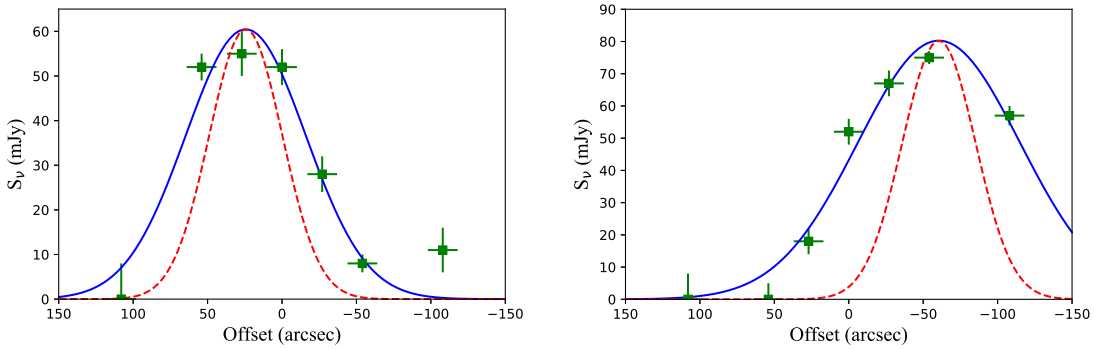

Figure 13. Same as Figure 11 but for 13.044 GHz SO (Table 4). Note that the SO emission is clearly extended.

transition.[12] We note that Mitchell et al. (1990) reported evidence for a two-temperature environment in NGC 7538 IRS1 (25 K and 176 K components). McCauley et al. (2011) argued that the 1 cm H_2CO absorption detected in their spectrum (see also our absorption detection in Figure 1) and the 2 cm H_2CO absorption reported by Hoffman et al. (2003) originate from the low temperature component. Our analysis is consistent with detection of high-density and warm-temperature molecular material, i.e., the transition region between the cold extended component (traced by 6 cm and 2 cm H_2CO absorption) and the NGC 7538 IRS1 hot and dense core traced by higher excitation transitions.

Although we use a simple non-LTE model, we can reliably conclude that the 2 cm H_2CO line in NGC 7538 IRS1 traces quasi-thermal emission, not a variable maser. We note that more complex models can be proposed to explain the results reported in this article. For example, several 2 cm masers separated by a few arcseconds would look like an extended source in our GBT cross-scan. However,

[12] McCauley et al. (2011) caution that their assumed temperature may not be correct but that the density determination is not greatly affected by temperature.

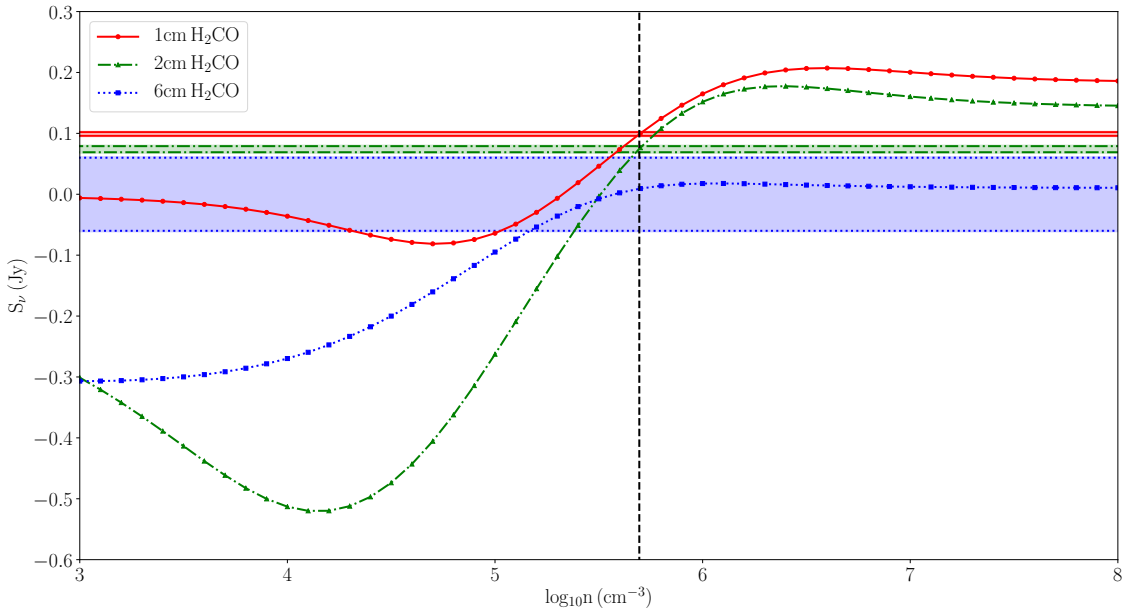

Figure 14. Predicted flux density of 1 cm (red, solid line), 2 cm (green, dot-dashed line) and 6 cm (blue, dotted line) H_2CO lines in NGC 7538 IRS1 as a function of density computed with RADEX. Shaded colour regions within horizontal lines (same line style mentioned above) show the range of observed flux density values including uncertainties (see Figure 1 and discussion in Section 4.3). We found that a density above 10^5 cm^{-3} (vertical dashed line) would result in flux density values for the three transitions that are consistent with our observations.

such masers would have to show simultaneous variability (to explain the non-detection by Hoffman et al. 2003), the masers would need to have a very similar LSR velocity (otherwise the emission line would be asymmetric or multi-peaked), and a similar maser distribution would be needed for the 1 cm transition (see Figure 1). Therefore, the simplest explanation is that 2 cm H_2CO traces extended, quasi-thermal emission that was resolved out by the VLA observations of Hoffman et al. (2003).

5 SUMMARY

We present observations conducted with the GBT of the 2 cm and 1 cm H_2CO lines toward NGC 7538 IRS1, which complement previous observations by our group of the 6 cm line. The observations were designed to investigate the nature of the 2 cm H_2CO emission in the region, as its velocity corresponds to the velocity of 6 cm H_2CO masers and also the systemic velocity of the thermal molecular gas. An East-West/North-South cross scan of the region revealed that the 2 cm H_2CO emission is tracing an extended molecular core ($\sim 50''$ in the East-West direction), which implies a low brightness temperature ($\sim$ 0.33 K). In addition, LTE and non-LTE analyses, including the 6 cm and 1 cm data, show that the 2 cm emission is not caused by a maser mechanism, but rather is a quasi-thermal line. Our analysis indicates that the 2 cm H_2CO emission originates from a dense ($\sim 10^5$ to 10^6 cm^{-3}) and warm ($\sim$ 40 K) molecular core, which marks the transition between the lower temperature/density extended molecular cloud (traced by 6 cm H_2CO absorption) and the hot and dense core in NGC 7538 IRS1 (traced by higher excitation transitions). Although this intermediate-temperature and high-density region is expected as molecular clouds collapse to form hot molecular cores, 2 cm H_2CO emission (like the one detected in this work) is rare. It is likely that in other regions the 2 cm H_2CO emission is engulfed (spectrally blended) with 2 cm H_2CO absorption from the most extended and lower-density gas, preventing detection of the emission. Given that both components (absorption and emission) are extended, detection of 2 cm H_2CO emission is challenging with interferometers, and therefore, single-dish high-angular resolution mapping is required to investigate this high-density warm-temperature transition envelope. Our work further exemplifies the potential of low K-doublet H_2CO observations as density probes in high-mass star forming regions as highlighted in the literature (e.g., McCauley et al. 2011).

ACKNOWLEDGEMENTS

E.D.A. acknowledges participation of Liang Yuan (WIU alumnus) in the initial stages of the data reduction and analysis of this project, that resulted in an AAS poster presentation (Yuan et al. 2011). E.D.A. also acknowledges partial support from NSF grant AST-1814063, and computational resources donated by the WIU Distinguished Alumnus Frank Rodeffer. P.H. acknowledges partial support from NSF grant AST-1814011. This article is based upon work supported by the Green Bank Observatory which is a major facility funded by the National Science Foundation operated by Associated Universities, Inc. The National Radio Astronomy Observatory (NRAO) is a facility of the National Science Foundation operated under cooperative agreement by Associated Universities, Inc. We acknowledge the careful revision and suggestions of an anonymous referee, which helped us to improve this article. This research has made use of NASA's Astrophysics Data System. This research has

made use of the NASA/IPAC Infrared Science Archive, which is funded by the National Aeronautics and Space Administration and operated by the California Institute of Technology.

DATA AVAILABILITY

The data underlying this article are available in the article and in its online Supporting Information.

REFERENCES

Akabane K., Inoue M., Kawabe R., Ohashi N., Kamaya O., Ishiguro M., Sofue Y., 1991, Proceedings of the Astronomical Society of Australia, 9, 118
Akabane K., Tsunekawa S., Inoue M., Kawabe R., Ohashi N., Kameya O., Ishiguro M., Sofue Y., 1992, PASJ, 44, 421
Andreev N., Araya E. D., Hoffman I. M., Hofner P., Kurtz S., Linz H., Olmi L., Lorran-Costa I., 2017, ApJS, 232, 29
Araya E., Hofner P., Kurtz S., Bronfman L., DeDeo S., 2005, ApJS, 157, 279
Araya E., Hofner P., Olmi L., Kurtz S., Linz H., 2006a, AJ, 132, 1851
Araya E., Hofner P., Goss W. M., Kurtz S., Linz H., Olmi L., 2006b, ApJ, 643, L33
Araya E., Hofner P., Goss W. M., Linz H., Kurtz S., Olmi L., 2007a, ApJS, 170, 152
Araya E., Hofner P., Goss W. M., 2007b, in Chapman J. M., Baan W. A., eds, IAU Symposium Vol. 242, Astrophysical Masers and their Environments. pp 110–119 (arXiv:0707.1841), doi:10.1017/S1743921307012653
Bastien P., Batrla W., Henkel C., Pauls T., Walmsley C. M., Wilson T. L., 1985, A&A, 146, 86
Ceccarelli C., Maret S., Tielens A. G. G. M., Castets A., Caux E., 2003, A&A, 410, 587
Chen X., et al., 2017a, MNRAS, 466, 4364
Chen X., Shen Z.-Q., Ellingsen S. P., Li X.-Q., Yang K., Chen H.-Y., Dong J., 2017b, ApJ, 851, L3
Evans N. J. I., Zuckerman B., Morris G., Sato T., 1975a, ApJ, 196, 433
Evans N. J. I., Zuckerman B., Sato T., Morris G., 1975b, ApJ, 199, 383
Galván-Madrid R., Montes G., Ramírez E. A., Kurtz S., Araya E., Hofner P., 2010, ApJ, 713, 423
Gaume R. A., Goss W. M., Dickel H. R., Wilson T. L., Johnston K. J., 1995, ApJ, 438, 776
Ginsburg A., Darling J., Battersby C., Zeiger B., Bally J., 2011, ApJ, 736, 149
Ginsburg A., et al., 2015, A&A, 584, L7
Ginsburg A., et al., 2016, A&A, 595, A27
Hoffman I. M., Goss W. M., Palmer P., Richards A. M. S., 2003, ApJ, 598, 1061
Johnston K. J., Henkel C., Wilson T. L., 1984, ApJ, 285, L85
Kameya O., Hasegawa T., Hirano N., Seki M., Tosa M., Taniguchi Y., Takakubo K., 1986, Ap&SS, 118, 449
Keown J., et al., 2019, ApJ, 884, 4
Luisi M., Anderson L. D., Balser D. S., Bania T. M., Wenger T. V., 2016, ApJ, 824, 125
Mangum J. G., Wootten A., 1993, ApJS, 89, 123
Mangum J. G., Darling J., Menten K. M., Henkel C., 2008, ApJ, 673, 832
McCauley P. I., Mangum J. G., Wootten A., 2011, ApJ, 742, 58
Minier V., Booth R. S., Conway J. E., 2002, A&A, 383, 614
Mitchell G. F., Maillard J.-P., Allen M., Beer R., Belcourt K., 1990, ApJ, 363, 554
Moscadelli L., Goddi C., 2014, A&A, 566, A150
Moscadelli L., Reid M. J., Menten K. M., Brunthaler A., Zheng X. W., Xu Y., 2009, ApJ, 693, 406
Ojha D. K., et al., 2004, ApJ, 616, 1042
Qiu K., Zhang Q., Menten K. M., 2011, ApJ, 728, 6
Sandell G., Sievers A., 2004, ApJ, 600, 269
Sandell G., Wright M., 2010, ApJ, 715, 919
Sandell G., Wright M., Zhu L., Zhao J.-H., Goss W. M., Corder S., 2012, The ionized jet and molecular outflow from NGC7538 IRS1, Poster presented at "ALMA/NAASC 2012 Workshop: Outflows, Winds and Jets", Charlottesville, Virginia, 3-6 March, 2012.
Sun Y., Gao Y., 2009, MNRAS, 392, 170
Thaddeus P., 1972, ApJ, 173, 317
Van der Tak F. F. S., van Dishoeck E. F., Evans Neal J. I., Blake G. A., 2000, ApJ, 537, 283
Van der Tak F. F. S., Black J. H., Schöier F. L., Jansen D. J., van Dishoeck E. F., 2007, A&A, 468, 627
Wright M. C. H., Hull C. L. H., Pillai T., Zhao J.-H., Sandell G., 2014, ApJ, 796, 112
Yuan L., Araya E. D., Hofner P., Kurtz S., Pihlstrom Y., 2011, in American Astronomical Society Meeting Abstracts #218. p. 129.04
Zheng X. W., Zhang Q., Ho P. T. P., Pratap P., 2001, ApJ, 550, 301

This paper has been typeset from a TEX/LATEX file prepared by the author.